Evidence for possible multiple chiral doublet bands with identical configuration in the odd-odd nucleus ^{126}Cs

T. J. Gao,[1] Jing-Bin Lu,[1,*] Yingjun Ma,[1] Yuhu Zhang,[2] S. Q. Zhang,[3] H. D. Wang,[1] Jia-Qiang Liu,[4] Pei-Yao Yang,[1] Zhen Ren,[1] Cheng-Qian Li,[1] Q. B. Chen,[5] Z. C. Gao,[6] Jian Li,[1] K. Y. Ma,[1] and Guoxiang Dong[7]

[1]*College of Physics, Jilin University, Changchun 130012, China*
[2]*Institute of Modern Physics, Chinese Academy of Sciences, Lanzhou 730000, China*
[3]*State Key Laboratory of Nuclear Physics and Technology, School of Physics, Peking University, Beijing 100871, China*
[4]*National Space Science Center Chinese Academy of Sciences, Beijing 101400, China*
[5]*Department of Physics, East China Normal University, Shanghai 200241, China*
[6]*China Institute of Atomic Energy, Beijing 102413, China*
[7]*School of Science, Huzhou University, Huzhou 313000, China*

(Received 14 September 2023; revised 7 December 2023; accepted 18 January 2024; published 7 February 2024)

A pair of new possible chiral doublet bands has been experimentally identified for the first time in the odd-odd nucleus ^{126}Cs. The possibility of multiple chiral doublet (MχD) bands in ^{126}Cs was interpreted by projected shell model (PSM) calculations with a relatively complete configuration space. The newly observed bands and the first chiral doublet band reported earlier belong to an identical configuration, providing the first experimental and theoretical evidence for the existence of multiple chiral doublet bands of odd-odd nuclei in the $A \approx 130$ mass region.

DOI: 10.1103/PhysRevC.109.024307

I. INTRODUCTION

Chiral symmetry breaking was first theoretically predicted for triaxial deformed nuclei in 1997 [1]. Much experimental evidence for chiral doublets has been reported in $A \approx$ 80, 100, 130, and 190 mass regions of the nuclear chart to date [2–5]. There may be multiple chiral doublet bands in the same nucleus, which is represented by the acronym MχD [6–10]. In recent years, Refs. [11–13] theoretically proposed the existence of multiple chiral doublet bands with identical configuration in odd-odd nuclei, which has been confirmed by experiments [14–16]. Theoretical studies of chiral doublet bands have been described by various approaches. The projected shell model (PSM) was also used to study the chiral geometry in numerous studies, and Refs. [17–20] obtained great results on Cs isotopes.

A pair of chiral doublet bands of ^{126}Cs has been studied previously [21–24]. In this paper, two new rotational bands labeled bands 3 and 4 and some linking transitions, which were observed for the first time in odd-odd nucleus ^{126}Cs in the $A \approx 130$ mass region, are established on the basis of the previous scheme. We use a projected shell model with a relatively complete configuration space to investigate the odd-odd nucleus ^{126}Cs in this work. The configuration of the four rotational bands of ^{126}Cs has been demonstrated as $\pi h_{11/2}^{1st} \otimes \nu h_{11/2}^{4th}$ by PSM. The energy spectrum and electromagnetic transition probabilities are reproduced for the four rotational bands. The chiral geometry of bands 1 and 2 as well as the evolution process of bands 3 and 4 in ^{126}Cs are illustrated for the first time by the distribution of the components of the angular momentum on the three intrinsic axes (K plot) and the distribution of the titled angles of the angular momentum in the intrinsic frame (*azimuthal* plot). The newly observed bands 3 and 4 are designated as a new possible chiral doublet band with the same configuration as the previously reported yrast and its partner band, which indicates the existence of multiple chiral doublet (MχD) bands in ^{126}Cs.

II. EXPERIMENTAL DETAILS

The γ-γ coincidence data reanalyzed in this work were collected earlier at NORDBALL by Komatsubara *et al.* [23]. A more complete level scheme was further deduced for ^{126}Cs in the present work, using the observed coincidence relations and relative intensities of the gamma transitions and based on the previously reported states for this nucleus. The partial level scheme for ^{126}Cs showing the bands relevant to the focus of this work is plotted in Fig. 1. Bands 1 and 2 were reported by Wang *et al.* in Ref. [21], while bands 3 and 4 are newly established on the basis of their level scheme in this work. At the same time, multiple intraband crossover transitions and interband transitions in both bands are established. Sample γ coincidence spectra, both gated by 141 keV, proving the placements of the levels in band 3 and 4, respectively, is displayed in Fig. 2. Spin assignments for new states are based on the ADO ratios (γ-ray angular distribution from oriented nuclei). In the present work, R_{ADO} values of $\approx$1.4 and $\approx$0.7 are expected for stretched quadrupole or $\Delta I = 0$ dipole radiations and stretched dipole transitions, respectively [21]. Taking a

*Corresponding author: ljb@jlu.edu.cn

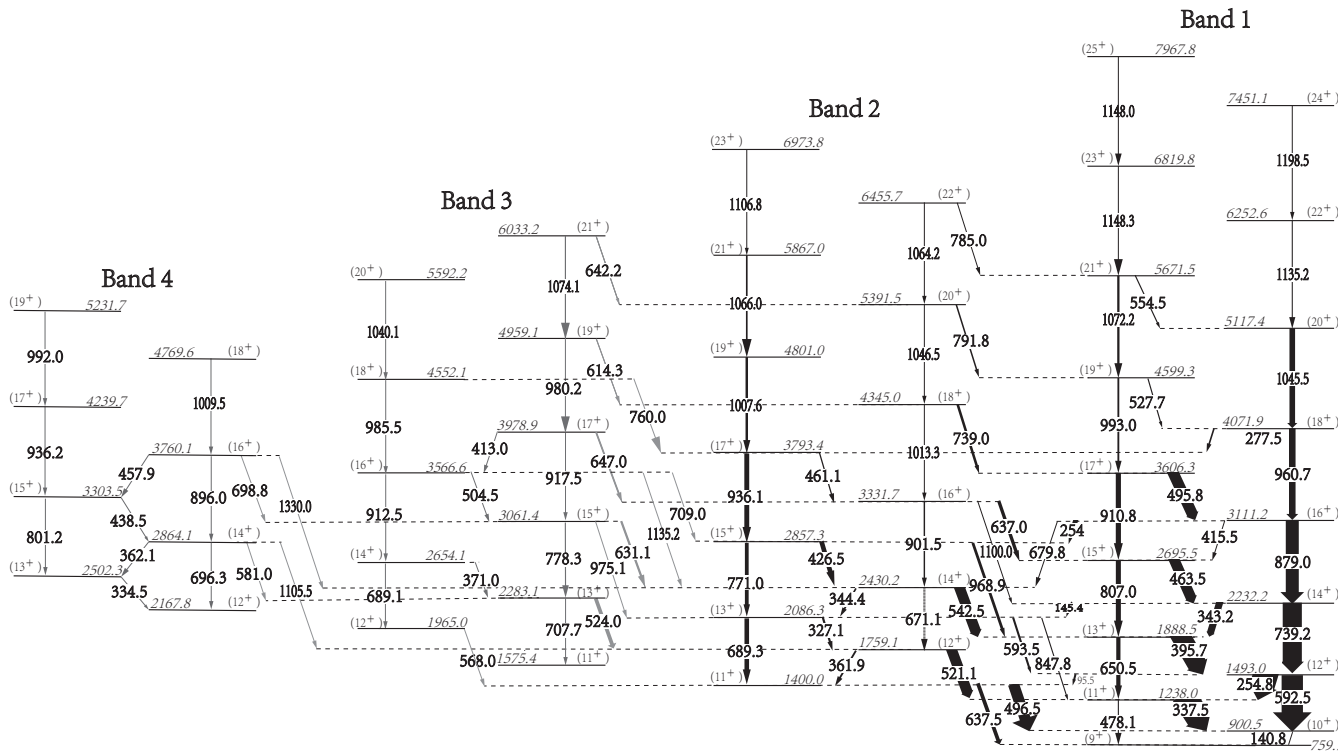

FIG. 1. Partial level scheme for ^{126}Cs. The energies are given in keV and the widths of the arrows are proportional to the relative transition intensities. All transitions within and outside band 3 (band 4) are shown in red (blue) color.

few strong transitions as an example, the 524 and 631 keV transitions connecting band 3 to band 2 were assigned $M1$ electromagnetic features based on ADO values of 0.75 and 0.69, respectively. Similarly, the 581 keV transition linking band 4 to band 3 is considered to be $M1$ character, based on an ADO value of 0.84. These dipole transitions fix the positive parity and the spin for bands 3 and 4. In conjunction with the deduced $M1$ multipolarity of the 524, 631, and 581 keV transitions, the two new bands are both specified as positive-parity bands. Bands 3 and 4 are both coupling bands of $\Delta I = 1$. Bands 1–4 all have positive parity and are linked to each other by many transitions. Moreover, the energy difference between the same spin levels is quite small. For the two pairs of bands 1 (3) and 2 (4), the energy difference values are both about 200 keV, and their $B(M1)/B(E2)$ values are extremely similar. These properties may indicate that the four bands in ^{126}Cs could correspond to two chiral doublet bands. The intensities and ADO coefficients for all newly observed rays are provided in Table I.

III. DISCUSSION

A. Projected shell model calculations

Calculations based on the projected shell model (PSM) were performed to investigate the properties of the four rotational bands. The PSM program improved in Refs. [18,19] is used in this paper, where quadrupole deformation

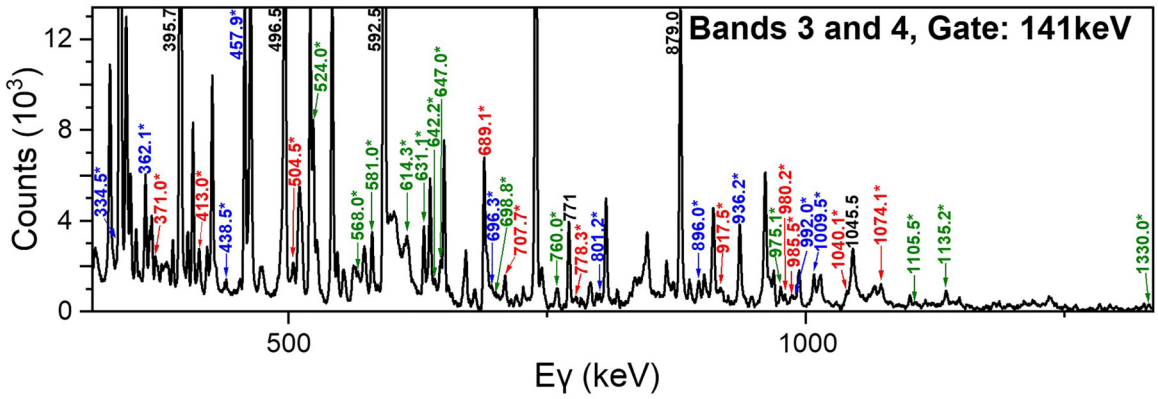

FIG. 2. Sample γ coincidence spectra gated by the 141 keV obtained in the present work showing the placement of the γ rays in bands 3 and 4. Transitions with band 3, band 4, and linking transitions are marked with stars, and labeled in red, blue, and green, respectively.

TABLE I. Energies, γ rays and ADO rations of γ rays in ^{126}Cs.

E_γ (keV)	I_γ (%)	ADO ratio	E_i (keV)	E_f (keV)	$I_i^\pi \to I_f^\pi$
Band 1					
140.8	100.0(3.0)	0.93(0.06)	900.5	759.7	$(10^+) \to (9^+)$
254.8	63.0(6.5)	0.70(0.08)	1493.0	1238.0	$(12^+) \to (11^+)$
337.5	62.2(3.8)	0.65(0.09)	1238.0	900.5	$(11^+) \to (10^+)$
343.2	17.8(2.6)	0.74(0.11)	2232.2	1888.5	$(14^+) \to (13^+)$
395.7	47.9(3.2)	0.66(0.08)	1888.5	1493.0	$(13^+) \to (12^+)$
415.5	2.5(0.4)		3111.2	2695.5	$(16^+) \to (15^+)$
463.5	26.7(2.5)	0.66(0.08)	2695.5	2232.2	$(15^+) \to (14^+)$
478.1	2.7(0.5)		1238.0	759.7	$(11^+) \to (9^+)$
495.8	15.6(3.3)	0.68(0.13)	3606.3	3111.2	$(17^+) \to (16^+)$
527.7	3.0(0.7)		4599.3	4071.9	$(19^+) \to (18^+)$
554.5	3.2(0.7)		5671.5	5117.4	$(21^+) \to (20^+)$
592.5	53.7(5.8)	1.36(0.19)	1493.0	900.5	$(12^+) \to (10^+)$
650.5	10.6(1.6)	1.44(0.35)	1888.5	1238.0	$(13^+) \to (11^+)$
739.2	48.2(5.5)	1.33(0.21)	2232.2	1493.0	$(14^+) \to (12^+)$
807.0	12.6(1.6)	1.34(0.27)	2695.5	1888.5	$(15^+) \to (13^+)$
879.0	32.7(1.7)	1.43(0.25)	3111.2	2232.2	$(16^+) \to (14^+)$
910.8	13.0(2.9)	1.39(0.27)	3606.3	2695.5	$(17^+) \to (15^+)$
960.7	16.5(3.5)	1.45(0.28)	4071.9	3111.2	$(18^+) \to (16^+)$
993.0	4.7(1.0)	1.46(0.46)	4599.3	3606.3	$(19^+) \to (17^+)$
1045.5	14.1(2.6)	1.63(0.34)	5117.4	4071.9	$(20^+) \to (18^+)$
1072.2	5.7(1.3)	1.27(0.35)	5671.5	4599.3	$(21^+) \to (19^+)$
1135.2	2.6(0.8)		6252.6	5117.4	$(22^+) \to (20^+)$
1148.0	1.0(0.3)		7967.8	6819.8	$(25^+) \to (23^+)$
1148.3	1.4(0.4)		6819.8	5671.5	$(23^+) \to (21^+)$
1198.5	1.0(0.3)		7451.1	6252.6	$(24^+) \to (22^+)$
Band 2					
327.1	4.6(0.6)	0.64(0.19)	2086.3	1759.1	$(13^+) \to (12^+)$
344.4	6.4(1.0)	0.71(0.22)	2430.2	2086.3	$(14^+) \to (13^+)$
361.9	4.7(0.8)	0.59(0.17)	1759.1	1397.0	$(12^+) \to (11^+)$
426.5	11.7(1.5)	0.66(0.16)	2857.3	2430.2	$(15^+) \to (14^+)$
461.1	3.2(0.7)		3793.4	3331.7	$(17^+) \to (16^+)$
671.1	5.7(0.8)	1.35(0.48)	2430.2	1759.1	$(14^+) \to (12^+)$
689.3	11.6(1.0)	1.37(0.28)	2086.3	1397.0	$(13^+) \to (11^+)$
771.0	9.4(1.2)	1.36(0.34)	2857.3	2086.3	$(15^+) \to (13^+)$
901.5	3.6(0.7)	1.44(0.48)	3331.7	2430.2	$(16^+) \to (14^+)$
936.1	12.3(2.3)	1.41(0.27)	3793.4	2857.3	$(17^+) \to (15^+)$
1007.6	6.2(1.5)	1.48(0.45)	4801.0	3793.4	$(19^+) \to (17^+)$
1013.3	1.6(0.5)		4345.0	3331.7	$(18^+) \to (16^+)$
1046.5	0.7(0.2)		5391.5	4345.0	$(20^+) \to (18^+)$
1064.2	0.6(0.2)		6455.7	5391.5	$(22^+) \to (20^+)$
1066.0	4.2(1.2)	1.51(0.46)	5867.0	4801.0	$(21^+) \to (19^+)$
1106.8	1.7(0.4)		6973.8	5867.0	$(23^+) \to (21^+)$
Band 3					
371.0	0.5(0.1)	0.70(0.10)	2654.1	2283.1	$(14^+) \to (13^+)$
413.0	1.5(0.1)	0.82(0.07)	3978.9	3566.6	$(17^+) \to (16^+)$
505.3	1.3(0.1)	0.66(0.23)	3566.6	3061.4	$(16^+) \to (15^+)$
689.1	0.7(0.1)	1.46(0.28)	2654.1	1965.0	$(14^+) \to (12^+)$
707.7	0.8(0.1)	1.37(0.20)	2283.1	1575.4	$(13^+) \to (11^+)$
778.3	1.1(0.1)	1.45(0.36)	3061.4	2283.1	$(15^+) \to (13^+)$
912.5	1.9(0.1)	1.21(0.25)	3566.6	2654.1	$(16^+) \to (14^+)$
918.0	2.2(0.1)	1.35(0.21)	3978.9	3061.4	$(17^+) \to (15^+)$
980.2	1.1(0.1)	1.36(0.42)	4959.1	3978.9	$(19^+) \to (17^+)$
985.5	1.3(0.1)	1.32(0.37)	4552.1	3566.6	$(18^+) \to (16^+)$
1040.1	0.2(0.1)	1.41(0.31)	5592.2	4552.1	$(20^+) \to (18^+)$
1074.1	0.1(0.1)	1.40(0.65)	6033.2	4959.1	$(21^+) \to (19^+)$

TABLE I. (*Continued*.)

E_γ (keV)	I_γ (%)	ADO ratio	E_i (keV)	E_f (keV)	$I_i^\pi \to I_f^\pi$
Band 4					
334.5	0.2(0.1)		2502.3	2167.8	$(13^+) \to (12^+)$
362.1	0.5(0.1)	0.84(0.14)	2864.1	2502.3	$(14^+) \to (13^+)$
438.5	0.7(0.1)	0.68(0.12)	3303.5	2864.1	$(15^+) \to (14^+)$
457.9	0.5(0.1)	0.63(0.05)	3760.1	3303.5	$(16^+) \to (15^+)$
696.3	0.7(0.1)	1.31(0.85)	2864.1	2167.8	$(14^+) \to (12^+)$
801.2	1.0(0.1)	1.35(0.16)	3303.5	2502.3	$(15^+) \to (13^+)$
896.0	1.2(0.1)	1.42(0.18)	3760.1	2864.1	$(16^+) \to (14^+)$
936.2	0.8(0.1)	1.47(0.39)	4239.7	3303.5	$(17^+) \to (15^+)$
992.0	0.5(0.1)	1.42(0.31)	5231.7	4239.7	$(19^+) \to (17^+)$
1009.5	0.8(0.1)	1.30(0.32)	4769.6	3760.1	$(18^+) \to (16^+)$
Linking transitions					
95.5	5.0(1.0)	0.94(0.26)	1493.0	1397.0	$(12^+) \to (11^+)$
145.4	3.7(0.6)	0.85(0.25)	2232.2	2086.3	$(14^+) \to (13^+)$
254.0	12.5(1.1)	0.69(0.13)	3111.2	2857.3	$(16^+) \to (15^+)$
277.5	4.1(1.1)	0.66(0.19)	4071.9	3793.4	$(18^+) \to (17^+)$
496.5	27.9(3.2)	0.59(0.08)	1397.0	900.5	$(11^+) \to (10^+)$
521.1	14.9(1.1)	0.72(0.08)	1759.1	1238.0	$(12^+) \to (11^+)$
524.0	8.6(0.1)	0.75(0.11)	2283.1	1759.1	$(13^+) \to (12^+)$
542.5	25.1(2.5)	0.64(0.06)	2430.2	1888.5	$(14^+) \to (13^+)$
568.0	1.1(0.1)	0.69(0.03)	1965.0	1397.0	$(12^+) \to (11^+)$
581.0	0.7(0.1)	0.84(0.09)	2864.1	2283.1	$(14^+) \to (13^+)$
593.5	5.3(0.9)	0.74(0.2)	2086.3	1493.0	$(13^+) \to (12^+)$
614.3	2.1(0.1)	0.71(0.05)	4959.1	4345.0	$(19^+) \to (18^+)$
631.1	5.9(0.1)	0.69(0.11)	3061.4	2430.2	$(15^+) \to (14^+)$
637.0	8.4(2.5)	0.66(0.14)	3331.7	2695.5	$(16^+) \to (15^+)$
637.5	9.4(2.6)	1.38(0.31)	1397.0	759.7	$(11^+) \to (9^+)$
642.2	0.9(0.1)	0.86(0.13)	6033.2	5391.5	$(21^+) \to (20^+)$
647.0	4.0(0.1)	0.63(0.05)	3978.9	3331.7	$(17^+) \to (16^+)$
679.8	2.1(0.6)		3111.2	2430.2	$(16^+) \to (14^+)$
698.8	0.8(0.1)	0.83(0.14)	3760.1	3061.4	$(16^+) \to (15^+)$
709.0	4.9(0.1)	0.80(0.11)	3566.6	2857.3	$(16^+) \to (15^+)$
739.0	6.4(1.5)	0.77(0.25)	4345.0	3606.3	$(18^+) \to (17^+)$
760.0	1.1(0.1)	0.91(0.11)	4552.1	3793.4	$(18^+) \to (17^+)$
785.0			6455.7	5671.5	$(22^+) \to (21^+)$
791.8	3.8(1.0)	0.72(0.21)	5391.5	4599.3	$(20^+) \to (19^+)$
847.8	2.7(0.9)		2086.3	1238.0	$(13^+) \to (11^+)$
968.9	7.0(2.1)	1.34(0.37)	2857.3	1888.5	$(15^+) \to (13^+)$
975.1	2.3(0.1)	1.35(0.23)	3061.4	2086.3	$(15^+) \to (13^+)$
1100.0	1.4(0.4)		3331.7	2232.2	$(16^+) \to (14^+)$
1105.5	0.4(0.1)	1.38(0.31)	2864.1	1759.1	$(14^+) \to (12^+)$
1136.0	1.9(0.1)	1.32(0.16)	3566.6	2430.2	$(16^+) \to (14^+)$
1330.0	0.4(0.1)	1.37(0.41)	3760.1	2430.2	$(16^+) \to (14^+)$

parameters (β, γ) are constrained at $(0.26, 24^\circ)$, consistent with the parameters used in the particle rotor model in Ref. [25], applied to the observed rotation band of the chiral nucleus ^{126}Cs.

B. Results and discussion

The results of the calculations in Fig. 3 are compared with our experimental data. For close excitation energies, an approximately constant staggering parameter $S(I)$, and a similar behavior of the $B(M1)/B(E2)$ ratios, are evident for both

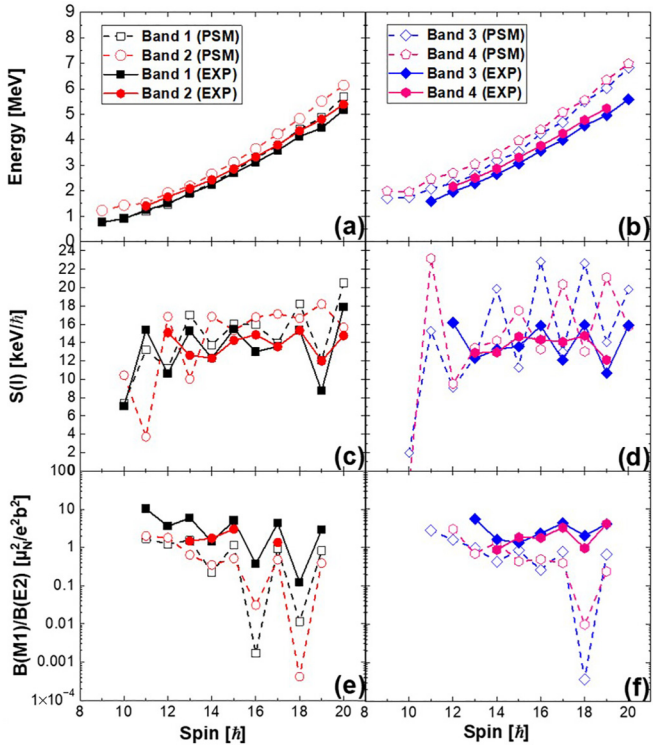

FIG. 3. (a),(b) Experimental excitation energies, (c),(d) $S(I)$ parameters, and (e),(f) $B(M1)/B(E2)$ ratios for the positive-parity chiral doublet in ^{126}Cs. Also shown are results of PSM calculations with the indicated deformation parameters.

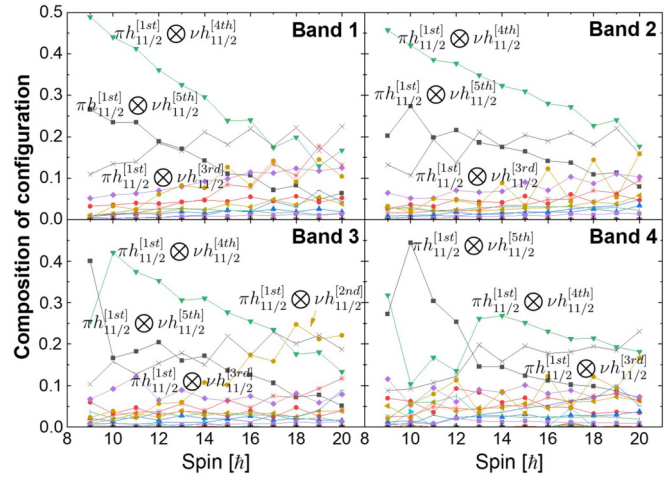

FIG. 4. Composition of configurations for bands 1–4. The corresponding configuration for each band is labeled by the same color.

chiral pairs. In Fig. 4, the compositions of configurations for band 1–4 are shown as functions of spin. For bands 1 and 2, the configuration $\pi h^{1st}_{11/2} \otimes \nu h^{4th}_{11/2}$ is dominant. For bands 3 and 4, the dominating configurations are also $\pi h^{1st}_{11/2} \otimes \nu h^{4th}_{11/2}$, but the configuration $\pi h^{1st}_{11/2} \otimes \nu h^{5th}_{11/2}$ strongly competes with $\pi h^{1st}_{11/2} \otimes \nu h^{4th}_{11/2}$.

The K distributions for the angular momentum on the three principal axes at the spins $I = 11\hbar$, $14\hbar$, $17\hbar$, and $20\hbar$ for bands 1–4 are shown in Figs. 5 and 6.

Bands 1 and 2. (i) For spin $I = 11\hbar$, the K plots shown in Fig. 5 are in accordance with the expectation for chiral vibration with respect to the s-l plane. The probability at $K_i = 0$ is significant for band 1, which corresponds to a zero-phonon state. On the other hand, the vanishing probability at $K_i = 0$ for band 2 indicates an antisymmetric wave function corresponding to a one-phonon state. (ii) For spin $I = 14\hbar$, the most probable value for K_i appears at $K_i \approx 12\hbar$ for band 1, which suggests that the collective rotation around the i axis develops and the angular momenta deviate from the s-l plane with the increase of spin. The peaks of the K_l and K_s distributions also correspond to K values substantially away from zero, so the most probable orientation of the angular momentum is aplanar. The K plots for band 2 are similar to those for band 1, supporting the occurrence of static chirality. (iii) For spins $I = 17\hbar$ and $20\hbar$, the K_s and K_l distributions become broad, and the peaks of the K_i distributions become sharp at $K_i \sim I$. Both features suggest that the angular momenta move close to the i axis, therefore the static chirality disappears.

Bands 3 and 4. (i) For spins $I = 11\hbar$ and $14\hbar$, there are two peaks at $K_i \approx 0\hbar$, $12\hbar$, and a node at $K_i \approx 6\hbar$ for band 3, corresponding to the two-phonon vibration. For band 4, there are two peaks at $K_i \approx 5\hbar$, $13\hbar$, and two nodes at $K_i \approx 0\hbar$, $10\hbar$, corresponding to three-phonon vibration. The K plots, shown in Fig. 6, are consistent with the expectation for chiral vibration with respect to the s-l plane. (ii) For spin $I = 17\hbar$, the chiral vibration for the two bands begins to disappear. The K_l distributions become broad, and the peaks of the K_i and K_s distributions become sharp at K_i and $K_s \sim I$. Both features suggest that the angular momenta move close to the i or s axis. (iii) For spin $I = 20\hbar$, the most probable values for K_i appear at $K_i \sim I$ for band 3, and collective rotation develops around the i axis. The most probable values for K_s appear at $K_s \sim I$ for band 4, and collective rotation develops around the s axis.

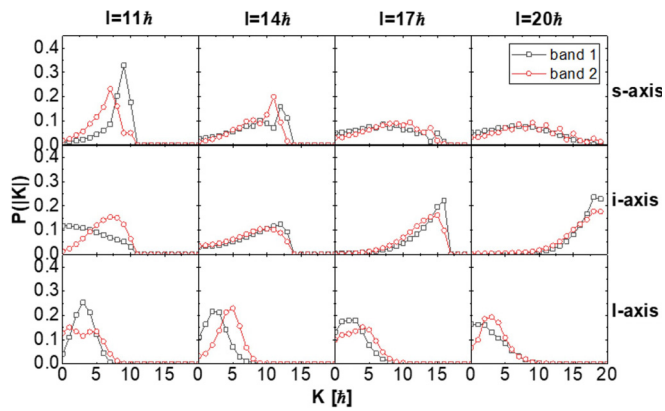

FIG. 5. The K plot, the K distributions for the angular momentum on the short (s), intermediate (i), and long (l) axes, calculated at spins $I = 11\hbar$, $14\hbar$, $17\hbar$, and $20\hbar$, respectively, for the chiral doublet bands 1 and 2 in ^{126}Cs.

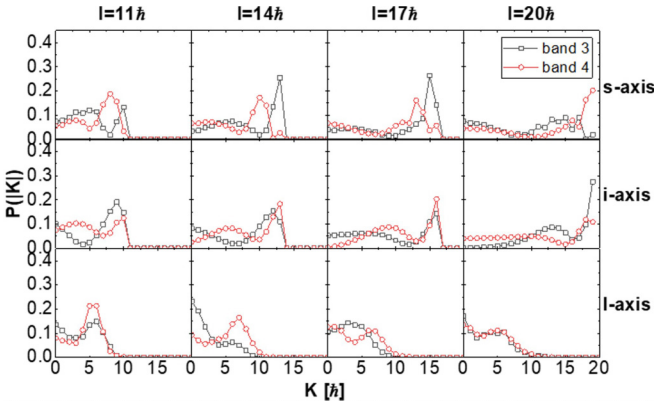

FIG. 6. The K plot, the K distributions for the angular momentum on the short (s), intermediate (i), and long (l) axes, calculated at spins $I = 11\hbar$, $14\hbar$, $17\hbar$, and $20\hbar$, respectively, for the bands 3 and 4 in ^{126}Cs.

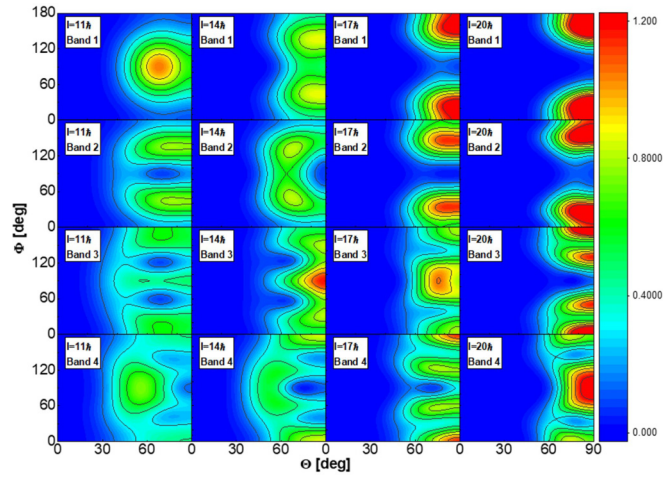

FIG. 7. The *azimuthal* plot, i.e., profile for the orientation of the angular momentum on the (θ, ϕ) plane, calculated at $I = 11\hbar$, $14\hbar$, $17\hbar$, and $20\hbar$ for bands 1–4 in ^{126}Cs.

In Fig. 7, the profiles for the orientation of the angular momentum on the (θ, ϕ) plane, the *azimuthal* plot, are shown for the same spins as in Figs. 5 and 6, respectively. The definitions of the angles (θ, ϕ) can be found in Refs. [18,19].

Bands 1 and 2. (i) For spin $I = 11\hbar$, the profiles for the orientation of the angular momentum for band 1 have a single peak at $(\theta \approx 70^\circ, \phi = 90^\circ)$, which suggests that the angular momentum stays within the s-l plane, in accordance with the expectation for a zero-phonon state. The profiles for band 2 show a node at $(\theta \approx 70^\circ, \phi = 90^\circ)$, with two peaks at $(\theta \approx 80^\circ, \phi \approx 45^\circ)$ and $(\theta \approx 80^\circ, \phi \approx 135^\circ)$, respectively, which supports the interpretation of a one-phonon vibration. Thus, the interpretation of chiral vibration is demonstrated. (ii) For spin $I = 14\hbar$, the *azimuthal* plots for bands 1 and 2 are similar. Two peaks corresponding to aplanar orientations are found, i.e., $(\theta \approx 80^\circ, \phi \approx 45^\circ)$ and $(\theta \approx 80^\circ, \phi \approx 135^\circ)$ for band 1, while $(\theta \approx 65^\circ, \phi \approx 45^\circ)$ and $(\theta \approx 65^\circ, \phi \approx 135^\circ)$ for band 2. These features can be understood as a realization of static chirality. (iii) For spins $I = 17\hbar$ and $20\hbar$, the peaks for the *azimuthal* plot for band 1 move toward $(\theta \approx 90^\circ, \phi \approx 20^\circ)$ and $(\theta \approx 90^\circ, \phi \approx 160^\circ)$, namely close to the i axis. It suggests the disappearance of the chiral geometry and the onset of principal axis rotation. The peaks for the *azimuthal* plot locate at $(\theta \approx 90^\circ, \phi \approx 25^\circ)$ and $(\theta \approx 90^\circ, \phi \approx 155^\circ)$ for band 2, which approach the i axis, meaning the chiral geometry is weakened.

Bands 3 and 4. (i) For spins $I = 11\hbar$ and $14\hbar$, the profiles for the orientation of the angular momentum for band 3 have three peaks and two nodes at $\theta \approx 65^\circ$, which suggests that the angular momentum stays within the s-l plane, in accordance with the expectation for a two-phonon vibration. On the other hand, the profiles for band 4 show three nodes at $\theta \approx 70^\circ$, with four peaks, supporting the interpretation of a three-phonon vibration. Thus, the interpretation of chiral vibration is demonstrated. (ii) For spin $I = 17\hbar$, there are three peaks located at $(\theta \approx 75^\circ, \phi = 90^\circ)$, $(\theta \approx 90^\circ, \phi = 0^\circ)$, and $(\theta \approx 90^\circ, \phi = 180^\circ)$ and two unclear nodes at $(\theta \approx 75^\circ, \phi \approx 35^\circ)$ and $(\theta \approx 75^\circ, \phi \approx 145^\circ)$ for band 3. There are four peaks located at $(\theta \approx 75^\circ, \phi \approx 55^\circ)$, $(\theta \approx 75^\circ, \phi \approx 125^\circ)$, $(\theta = 90^\circ, \phi = 0^\circ)$, and $(\theta = 90^\circ, \phi = 180^\circ)$, one clear node at $(\theta \approx 70^\circ, \phi = 90^\circ)$, and two unclear nodes at $(\theta \approx 70^\circ, \phi \approx 30^\circ)$ and $(\theta \approx 70^\circ, \phi \approx 150^\circ)$ for band 4, which means that the chiral vibration is disappearing. (iii) For spins $I = 20\hbar$, there are two peaks at $(\theta = 90^\circ, \phi = 0^\circ)$ and $(\theta = 90^\circ, \phi = 180^\circ)$ for band 3, and collective rotation develops around the i-axis; and there is one peak at $(\theta = 90^\circ, \phi = 90^\circ)$ for band 4, and collective rotation develops around the s-axis.

IV. CONCLUSION

In summary, in addition to the yrast and its partner band previously reported, a new pair of chiral doublet bands based on the two-quasiparticle $\pi h_{11/2}^{1st} \otimes \nu h_{11/2}^{4th}$ configuration has been identified in odd-odd nucleus ^{126}Cs belonging to $A \approx 130$. The experimental data have been compared with the results of the projected shell model with a complete configuration space. The evolution from chiral vibration to static chiral rotation for bands 1 and 2 as well as the evolution of bands 3 and 4 in ^{126}Cs were also investigated for the first time in this paper. The chiral geometry with bands 3 and 4 is not typical due to the high excitation energy and the mixed configuration, and thus exhibits more chiral vibrational features. All these results provide theoretical and experimental evidence for the possible existence of MχD with the identical configuration in the odd-odd nucleus ^{126}Cs in the $A \approx 130$ mass region.

ACKNOWLEDGMENTS

We thank T. Komatsubara for providing the experimental data of ^{126}Cs. We thank J. Meng for his discussion regarding this work, as well as F.Q. Chen and Y.K. Wang for providing the projected shell model program and guidance on theoretical calculations. This study was supported by the National Natural Science Foundation of China (Grants No. U1867210 and No. 12205103).

[1] S. Frauendorf and J. Meng, Nucl. Phys. A **617**, 131 (1997).
[2] C. Liu, S. Y. Wang, R. A. Bark, S. Q. Zhang, J. Meng, B. Qi *et al.*, Phys. Rev. Lett. **116**, 112501 (2016).
[3] P. Joshi, M. P. Carpenter, D. B. Fossan, T. Koike, E. S. Paul, G. Rainovski, K. Starosta, C. Vaman, and R. Wadsworth, Phys. Rev. Lett. **98**, 102501 (2007).
[4] D. Tonev, G. de Angelis, P. Petkov, A. Dewald, S. Brant, S. Frauendorf *et al.*, Phys. Rev. Lett. **96**, 052501 (2006).
[5] D. L. Balabanski, M. Danchev, D. J. Hartley, L. L. Riedinger, O. Zeidan, J.-Y. Zhang *et al.*, Phys. Rev. C **70**, 044305 (2004).
[6] J. Meng, J. Peng, S. Q. Zhang, and S.-G. Zhou, Phys. Rev. C **73**, 037303 (2006).
[7] A. D. Ayangeakaa, U. Garg, M. D. Anthony, S. Frauendorf, J. T. Matta, B. K. Nayak *et al.*, Phys. Rev. Lett. **110**, 172504 (2013).
[8] J. Peng, H. Sagawa, S. Q. Zhang, J. M. Yao, Y. Zhang, and J. Meng, Phys. Rev. C **77**, 024309 (2008).
[9] J. Li, S. Q. Zhang, and J. Meng, Phys. Rev. C **83**, 037301 (2011).
[10] J. M. Yao, B. Qi, S. Q. Zhang, J. Peng, S. Y. Wang, and J. Meng, Phys. Rev. C **79**, 067302 (2009).
[11] I. Hamamoto, Phys. Rev. C **88**, 024327 (2013).
[12] C. Droste, S. G. Rohoziński, K. Starosta, L. Pròchniak, and E. Grodner, Eur. Phys. J. A **42**, 79 (2009).
[13] Q. B. Chen, J. M. Yao, S. Q. Zhang, and B. Qi, Phys. Rev. C **82**, 067302 (2010).
[14] B. Qi, H. Jia, N. B. Zhang, C. Liu, and S. Y. Wang, Phys. Rev. C **88**, 027302 (2013).
[15] S.-Y. Wang, Chin. Phys. C **44**, 112001 (2020).
[16] I. Kuti, Q. B. Chen, J. Timàr, D. Sohler, S. Q. Zhang, Z. H. Zhang, P. W. Zhao, J. Meng, K. Starosta, T. Koike, E. S. Paul, D. B. Fossan, and C. Vaman, Phys. Rev. Lett. **113**, 032501 (2014).
[17] Z.-C. Gao, Y. S. Chen, and Y. Sun, Phys. Lett. B **634**, 195 (2006).
[18] F. Q. Chen, J. Meng, and S. Q. Zhang, Phys. Lett. B **785**, 211 (2018).
[19] F. Q. Chen, Q. B. Chen, Y. A. Luo, J. Meng, and S. Q. Zhang, Phys. Rev. C **96**, 051303(R) (2017).
[20] G. H. Bhat, J. A. Sheikh, and R. Palit, Phys. Lett. B **707**, 250 (2012).
[21] S. Y. Wang, Y.-Z. Liu, T. Komatsubara, Y. J. Ma, and Y. Zhang, Phys. Rev. C **74**, 017302 (2006).
[22] S. Y. Wang, S.-Q. Zhang, B. Qi, and J. Meng, Chin. Phys. Lett. **24**, 536 (2007).
[23] T. Komatsubara, K. Furuno, T. Hosoda, J. Mukai, T. Hayakawa, T. Morikawa *et al.*, Nucl. Phys. A **557**, 419 (1993).
[24] E. Grodner, I. Sankowska, T. Morek, S. G. Rohoziński, C. Droste, J. Srebrny *et al.*, Phys. Lett. B **703**, 46 (2011).
[25] S. Y. Wang, S. Q. Zhang, B. Qi, and J. Meng, Phys. Rev. C **75**, 024309 (2007).